How to cite: Angew. Chem. Int. Ed. 2023, e202306890
doi.org/10.1002/anie.202306890

Nanographenes

Extension of Non-alternant Nanographenes Containing Nitrogen-Doped Stone-Thrower-Wales Defects

*Chang Wang, Ziqi Deng, David Lee Phillips, and Junzhi Liu**

Abstract: Non-alternant topologies have attracted considerable attention due to their unique physiochemical characteristics in recent years. Here, three novel topological nanographenes molecular models of nitrogen-doped Stone–Thrower–Wales (S–T–W) defects were achieved through intramolecular direct arylation. Their chemical structures were unambiguously elucidated by single-crystal analysis. Among them, threefold intramolecular direct arylation compound ($C_{42}H_{21}N$) is the largest nanographene bearing a N-doped non-alternant topology to date, in which the non-benzenoid rings account for 83 % of the total molecular skeleton. The absorption maxima of this compound was located in the near-infrared region with a long tail up to 900 nm, which was much longer than those reported for similarly sized N-doped nanographene with six-membered rings ($C_{40}H_{15}N$). In addition, the electronic energy gaps of these series compounds clearly decreased with the introduction of non-alternant topologies (from 2.27 eV to 1.50 eV). It is noteworthy that $C_{42}H_{21}N$ possesses such a low energy gap ($E_g^{opt}=1.40$ eV; $E_g^{cv}=1.50$ eV), yet is highly stable under ambient conditions. Our work reported herein demonstrates that the non-alternant topology could significantly influence the electronic configurations of nanocarbons, where the introduction of a non-alternanting topology may be an effective way to narrow the energy gap without extending the molecular π-conjugation.

[*] C. Wang, Z. Deng, Prof. Dr. D. L. Phillips, Dr. J. Liu
Department of Chemistry and State Key Laboratory of Synthetic Chemistry, The University of Hong Kong
Pokfulam Road, Hong Kong 999077 (China)
E-mail: juliu@hku.hk

C. Wang
Chemistry and Chemical Engineering Guangdong Laboratory, Shantou, 515031, China

Introduction

Non-alternant-embedded nanographenes, which exhibit entirely different electronic and optical properties from their corresponding alternant systems, have attracted considerable attention in recent years due to their unique molecular orbital distributions.[1–9] For instance, the antiaromatic characteristics, anti-Kasha and open shell features of π-extended nanographenes with azulene or pentalene units have been developed.[10–15] However, apart from these azulene or pentalene moieties, research on larger non-alternant structures is rare due to the challenges of in-solution synthesis. In the middle of the 19th century, different types of non-alternant molecules, such as azupyrene (the isomer of alternant pyrene, also called Stone–Thrower–Wales (S–T–W) defect in graphene, Figure 1a) and dicycloheptapentalene (also called the inverse S–T–W defect in graphene, Figure 1a), were synthesized.[16–18] However, since Anderson and co-workers reported the first synthesis and characterization of azupyrene in 1968, the synthesis of π-expanded nanographenes containing azupyrene unit has remained elusive in recent decades, likely owing to the lack of a facile synthetic approach and ring rearrangement.[16,17,19] Consequently, the physicochemical properties induced by this topological S–T–W defect in graphene nanostructures are difficult to ascertain. Nevertheless, it is possible to induce unique physicochemical properties when integrating such non-alternant topologies in graphene molecules.[20–26] For instance, the curvature, aromaticity, chemical activities, and optical properties of nanographenes could be affected by the introduction of S–T–W defect.[20–27] A case in point is the only experimental synthesis of π-extended azupyrene-embedded nanographene reported by Konishi and Yasuda in 2019 (Figure 1a), which demonstrated unique open-shell characteristic.[27] Most recently, Morin's group reported the synthesis of π-expanded inverse S–T–W defect (Figure 1a).[28] Nevertheless, integrating the edge-sharing pentagon and heptagon into the polyarene framework is a very challenging task due to a lack of appropriate synthetic methodologies to form more than four nonhexagonal rings in the same molecule.

Introducing of heteroatoms into polycyclic aromatic structures is another strategy to alter their intrinsic optoelectronic properties.[29–32] Among the heteroatoms, nitrogen (N) plays an important role in modulating the electronic characteristics of π-conjugated architectures due to its electron accepting and donating abilities based on the different hybrid orbital bonding manners.[33–35] However, the synthetic strategies of π-extended systems usually require

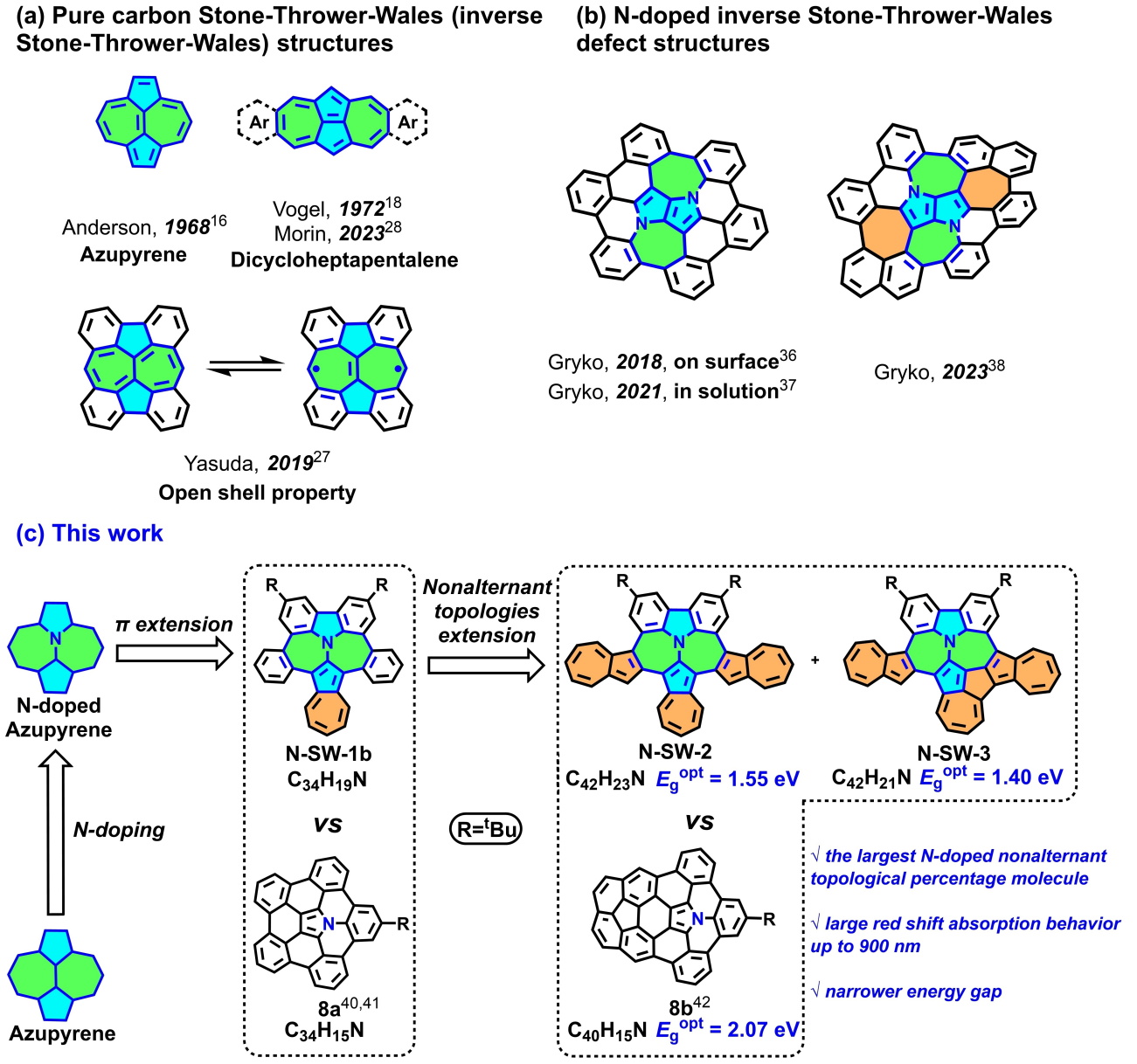

Figure 1. (a) Examples of pure carbon molecules with S–T–W (or inverse S–T–W) defect. (b) Specific examples of nanographenes with N-doped inverse S–T–W defects. (c) Our work on nanographenes containing an N-doped S–T–W defect and further extension of the non-alternant topologies.

high temperature reaction conditions, which few heterocycles can tolerate, thus hindering the development of N-embedded nanographenes bearing non-alternant topologies.[33–36] In 2018, Gryko's group first synthesized a N-doped nanographene with an inverse S–T–W defect on the surface and confirmed the molecular constitution using bond-resolved scanning tunneling microscopy (Figure 1b).[36] In 2021, the same group successfully synthesized the same core structure in solution using direct arylation and characterized its fundamental optical and electronic properties.[37] Very recently, this group introduced two additional heptagons into the molecular skeleton (Figure 1b).[38] Despite the swift development of N-doped polycyclic hydrocarbons in recent years, to the best of our knowledge, nanographenes bearing N-doped S–T–W defect have yet to be extensively investigated, and there is still a very large uncharted territory to be explored.[39]

Here, using azulene and carbazole units as the starting building blocks, three novel saddle-shaped nanographenes (**N-SW-1**, **N-SW-2** and **N-SW-3**, Figure 1c and Scheme 1) were successfully obtained through intramolecular direct arylation in solution. The structure containing two adjacent N-doped heptagons between two pentagons could be identified as N-doped Stone-Thrower-Wales defect in graphene. Interestingly, compounds **N-SW-2** ($C_{42}H_{23}N$) and **N-SW-3** ($C_{42}H_{21}N$) exhibited long absorption tails up to the near-infrared region (900 nm), compared to those reported for similarly sized N-doped nanographene with six-mem-

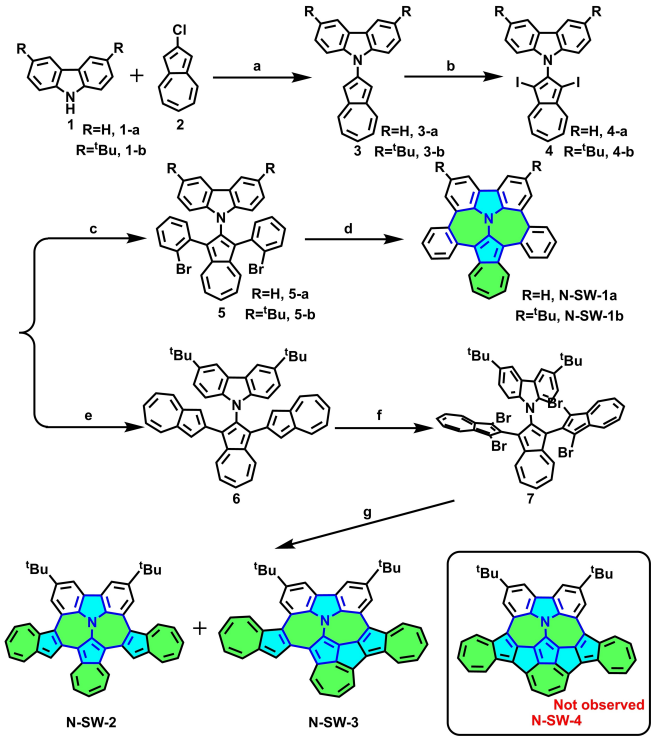

Scheme 1. Synthetic routes to the **N-SW** series of non-alternant nanographenes. Reagents and conditions: (a) $Pd_2(dba)_3$, S–Phos, ^{t}BuONa, toluene, 110 °C, 24 h, 45 % and 83 % yields for R=H and R=^{t}Bu, respectively; (b) NIS, DCM, 0 °C, 1 h, 80 % and 93 % yields for R=H and R=^{t}Bu, respectively; (c) (2-bromophenyl)boronic acid, Pd(dppf)Cl_2, Na_2CO_3, DMSO, H_2O, 70 °C, 20 h, 15 % and 18 % yields for R=H and R=^{t}Bu, respectively; (d) $Pd(OAc)_2$, $PCy_3.BF_4$, PivOH, K_2CO_3, DMA, 145 °C, 20 h, 23 % and 26 % yields for R=H and R=^{t}Bu, respectively; (e) 2-(4,4,5,5-tetramethyl-1,3,2-dioxa-borolanyl)azulene, Pd(dppf)Cl_2, Na_2CO_3, dioxane, H_2O, 80 °C, 20 h, 43 %; (f) NBS, DCM, 0 °C, 1 h, 65 %; (g) $Pd(OAc)_2$, $PCy_3.BF_4$, PivOH, K_2CO_3, DMA, 115 °C, 20 h, 10 % for **N-SW-2** and 3 % for **N-SW-3**. Abbreviations: $Pd_2(dba)_3$, tris(dibenzylideneacetone)dipalladium(0); S-Phos, 2-dicyclohexylphosphino-2′,6′-dimethoxybiphenyl; tBuONa, sodium tert-butoxide; NIS, *N*-iodosuccinimide; DCM, dichloromethane; Na_2CO_3, sodium carbonate; DMSO, dimethyl sulfoxide; $Pd(OAc)_2$, palladium(II) acetate; Pd(dppf)Cl_2, [1,1′-bis(diphenylphosphino)ferrocene]dichloropalladium(II); K_2CO_3, potassium carbonate; DMA, *N*,*N*-dimethylacetamide; $PCy_3.BF_4$, tri(cyclohexyl)phosphine tetrafluoroborate; NBS, *N*-bromosuccinimide; PivOH, pivalic acid.

bered rings (**8b**[42] ($C_{40}H_{15}N$) in Figure 1c, which showed UV absorption at 400–600 nm).[40–42] Remarkably, compound **N-SW-3** possesses such a low energy gap (E_g^{opt} = 1.40 eV), yet is highly stable under ambient conditions (Figure S41). Our work provides a rational strategy to synthesize nanographenes with π-expanded non-alternant topologies, in which the introduction of a non-alternant topology might be a promising way to narrow the energy gap without extending the molecular π-conjugation.

Results and Discussion

Carbazole is a commercially available heterocycle that has a N-doped five-membered ring. Through the Buchwald–Hartwig reaction with **1-a** (**1-b**) and **2**, **3-a** and **3-b** with two five-membered rings were obtained in 45 % and 83 % yields, respectively (Scheme 1). Then, iodination of the **3**-series using N-iodosuccinimide (NIS) provided **4-a** and **4-b** in yields in 80 % and 93 %, respectively. The Suzuki–Miyaura reaction of **4**-series and (2-bromophenyl)boronic acid gave bromo-substituted compounds **5-a** and **5-b** in 15 % and 18 % yields, respectively. Finally, the target compounds **N-SW-1a** and **N-SW-1b** were synthesized by utilizing intramolecular direct arylation with the yields of 23 % and 26 %, respectively. Furthermore, compound **6** with three azulene units was obtained in the yield of 43 % through Suzuki–Miyaura coupling of 2-(4,4,5,5-tetramethyl-1,3,2-dioxaborolanyl)azulene[43] and **4-b**. Thereafter, bromination of **6** offered **7** in 65 % yield. Further intramolecular direct arylation successfully achieved the molecules **N-SW-2** and **N-SW-3** with π-expanded non-alternant topologies. However, fully fused nanographene **N-SW-4** was not observed (Scheme 1), this is likely due to the debromination of the substrate and the large strain after the formation of **N-SW-3**. The chemical structures of **N-SW-1**, **N-SW-2** and **N-SW-3** were characterized by HR-MS, ^{1}H NMR, ^{13}C NMR (Supporting Information) and single crystal analysis (Figure 2).

Single crystals[44] of **N-SW-1a**, **N-SW-2** and **N-SW-3** were obtained by slowly evaporating them from DCM/methanol (MeOH), DCM/MeOH and carbon disulfide (CS_2)/hexane, respectively. The top view structures of **N-SW-1a**, **N-SW-2** and **N-SW-3** are shown in Figure 2a–2c, which unambiguously confirmed the non-alternant topologies. With π-system extension, the dihedral angles between the mean planes of the terminal rings became narrower. All of the **N-SW** series displayed saddle-shaped conformations. The presence of symmetric cove edges with *M*- and *P*-chirality around N-doped heptagons make **N-SW-1a** and **N-SW-2** chiral with mesomeric properties of *M/P* and *M/P/P/M* configurations. **N-SW-3** showed enantiomer pair (*M/P/P*)-**N-SW-3** and (*P/M/M*)-**N-SW-3** in one unit cell because of the asymmetrical conformation. The flip energy barriers of these three compounds were 14.94 kcal/mol for **N-SW-1**, 14.37 kcal/mol for **N-SW-2** and 7.81 kcal/mol for **N-SW-3** (Figure S47), respectively, which estimated by time-dependent density functional theory (TD-DFT) calculations at the B3LYP-311G(d,p) level of theory. These theoretical results demonstrated that all these three compounds could flip freely at room temperature.[5a] The distances from the bottom side carbon atom in the azulene unit to the middle of the top side carbon atom in the carbazole unit of **N-SW-1a** and **N-SW-2** were 9.15 Å and 9.38 Å (Figure 2a and 2b), respectively. The distances from the carbon atom in the azulene unit and the carbon atom in the carbazole unit to the middle section plane of **N-SW-1a** are longer than those of **N-SW-2**, indicating the planar tendency induced by increasing π-conjugation. As shown in Figure S39, the bond length distributions of the N-doped azupyrene structures in **N-SW-1a** and **N-SW-2** were quite similar, with identical alternant

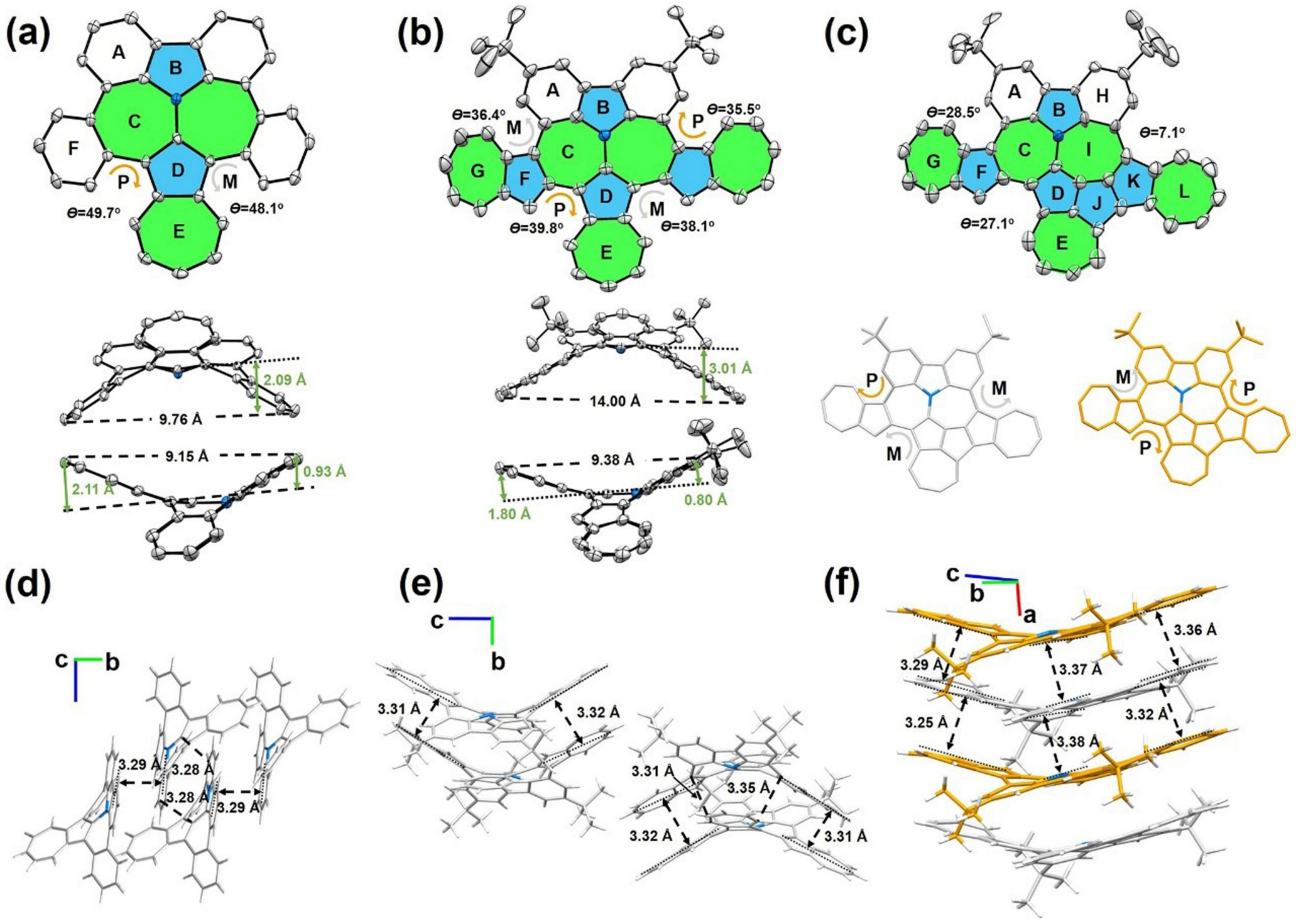

Figure 2. X-ray crystal structures of **N-SW-1a**, **N-SW-2** and **N-SW-3**. (a) Top view (convex face, up) and side view (down) of **N-SW-1a**. (b) Top view (convex face, up) and side view (down) of **N-SW-2**. (c) Top views (convex face) of **N-SW-3** (up) and its enantiomer pairs (down) in the crystal unit cell. (d) Selected packing structures of **N-SW-1a** along different views. (e) Selected packing structures of **N-SW-2** along different views. (f) Selected packing structures of **N-SW-3** along different views.

bond length trends in N-doped heptalenes, suggesting antiaromatic properties in these two N-doped heptagons, which were quite consistent with the results of NICS calculations. The bond length distributions in **N-SW-3**, however, were totally different from those in **N-SW-2**. The bond length trends in the two N-doped heptagons (C and I rings) in **N-SW-3** (Figure S39c) became asymmetrical compared with those in **N-SW-2**. In addition, only the left side azulene unit[45] (F and G rings) retained azulene bond length properties in **N-SW-3**, while all of the peripheral azulene units in **N-SW-2** displayed azulene bond length characteristics. The doubtless single bond (1.52 Å) appearing in the extra fusing pentagon (J ring) in **N-SW-3** might change the aromatic characteristics of the whole structure. The J ring, thereafter, could be regarded as an additional antiaromatic ring in **N-SW-3** and as the crucial part to break the symmetry of the molecule.

In the solid-state, as shown in Figure 2d–2f and Figure S40, **N-SW-1a** and **N-SW-2** were packed in a sandwich herringbone model, while **N-SW-3** exhibited a sheet-style packing structure. **N-SW-1a** demonstrated a head-to-head packing model with a π–π stacking distance of 3.29 Å between two intermolecular carbazole units and a head-to-tail π–π stacking distance of 3.28 Å between the carbazole unit (head) and azulene unit (tail) (Figure 2d). **N-SW-1a** was also arranged via C–H···π interactions with distances of 2.85 Å–2.89 Å and van der Waals dispersion forces (vdW forces) with distances of 2.26 Å–2.37 Å from the top view (Figure S40a). **N-SW-2** was arranged with two head-to-tail modes in one crystal cell unit with π–π stacking distances of 3.31 Å–3.35 Å (Figure 2e). From the top view, **N-SW-2** was packed via intermolecular vdW forces with a distance of 2.32 Å (Figure S40b). **N-SW-3** was packed via head-to-tail modes with π–π stacking distances of 3.29 Å–3.37 Å and 3.25 Å–3.38 Å induced by alternant *P/M/M* and *M/P/P* conformations (Figure 2f). From the top view, **N-SW-3** was packed via intermolecular vdW forces with distances of 2.34 Å–2.38 Å (Figure S40c).

UV–Vis absorption spectra of **N-SW-1b**, **N-SW-2** and **N-SW-3** were all determined in DCM to compare the influence of non-alternant topologies (Figure 3a). The stabilities of the **N-SW** series were monitored via the time-dependent UV–Vis absorption. Their absorption peaks barely changed after 50 days (Figure S41), indicating that these non-alternant

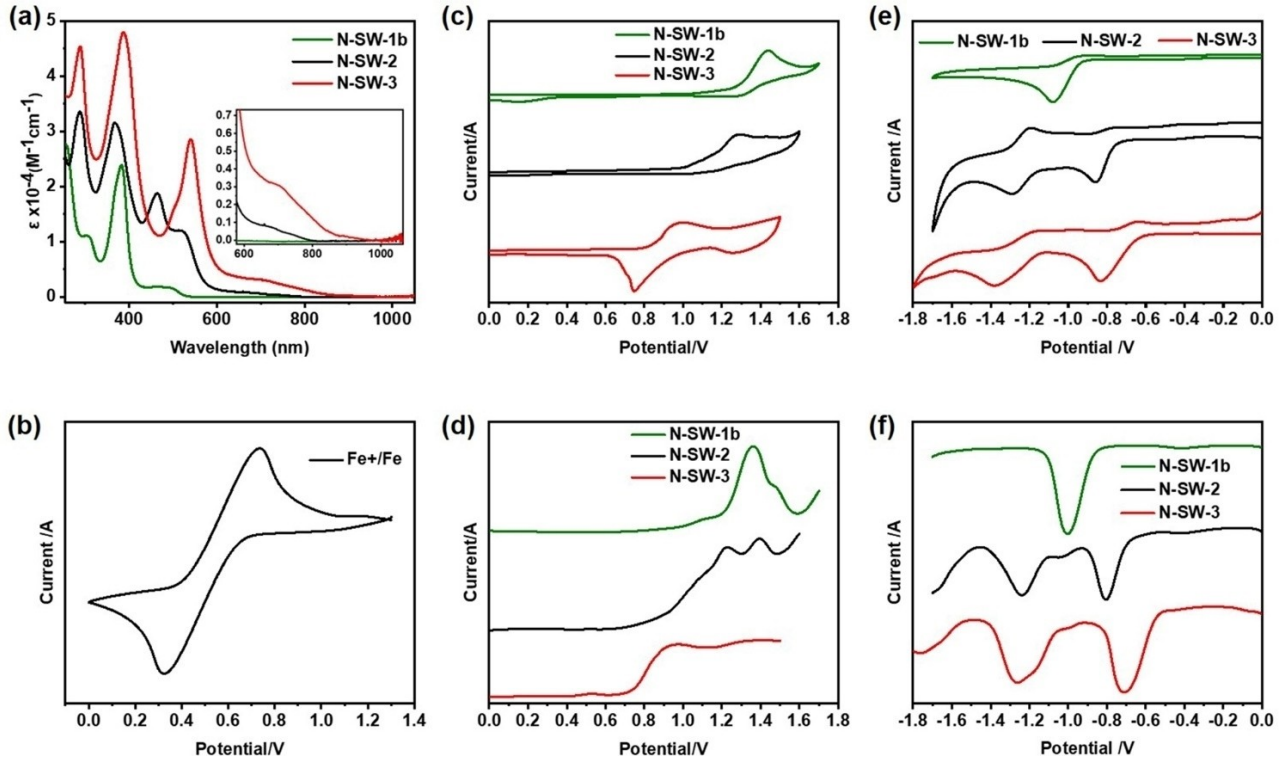

Figure 3. (a) UV–Vis absorption spectra of the **N-SW** series in DCM. (b) CV of Ferrocene (Fc) in THF, the onset oxidation potential of Fc was 0.42 V (E_{Fc} = 0.42 eV). CV (c) and DPV (d) spectra of oxidation region measured in THF. CV (e) and DPV (f) spectra of the reduction region measured in THF. Scan rate: 0.05 V/s. All the CV data was measured with 0.1 M Bu_4NPF_6 in THF.

nanographenes are highly stable under ambient conditions. As shown in Figure 3a, **N-SW-1b** displayed two distinct absorption peaks at 260 nm and 380 nm with molar extinction coefficients (ε) at 27500 $M^{-1}cm^{-1}$ and 23900 $M^{-1}cm^{-1}$, respectively. **N-SW-1b** also displayed two obvious shoulder peaks at 300 nm and 480 nm. Based on TD-DFT calculations at B3LYP/6-311G(d,p) level (Figure S46a and table S1), the peak at 380 nm of **N-SW-1b** was belong to higher excitation transitions (S_0 to S_6). For **N-SW-2**, the UV–Vis spectrum displayed three peaks at approximately 290 nm (ε: 33500 $M^{-1}cm^{-1}$), 365 nm (ε: 31600 $M^{-1}cm^{-1}$) and 465 nm (ε: 18700 $M^{-1}cm^{-1}$, contributed by S_0 to S_8 and S_9 transitions, shown in Figure S46b and table S2), as well as one shoulder peak from 500 nm to 525 nm, and a long tail peak up to 800 nm (belong to the transition from S_0 to S_1 and S_2). In contrast, for **N-SW-3**, the UV–Vis spectrum only showed three peaks at approximately 290 nm (ε: 45400 $M^{-1}cm^{-1}$), 387 nm (ε: 47900 $M^{-1}cm^{-1}$) and 543 nm (ε: 28500 $M^{-1}cm^{-1}$, contributed by S_0 to S_6 and S_7 transitions, depicted in Figure S46c and table S3) along with a longer tail peak up to 900 nm (belong to the transition from S_0 to S_1, S_2 and S_3). The optical energy gaps of these series were 2.34 eV for **N-SW-1b**, 1.55 eV for **N-SW-2** and 1.40 eV for **N-SW-3** based on their absorptions onset (λ_{onset}). Meanwhile, the **N-SW** series molecules displayed no emission characteristics based on the fluorescent spectra in DCM (Figure S43 and Figure S44). These values are consistent with the results of their electrical energy gaps, suggesting that narrower energy gaps can be achieved with extension of the non-alternant topology compared with that of similarly sized N-doped nanographene with six-membered rings (E_g^{opt} = 2.07 eV for **8b**[42] ($C_{40}H_{15}N$), Figure 1c). The great stability of **N-SW-3** with a narrower energy gap indicated that the incorporation of non-alternant topology into nanographenes might be a reasonable strategy for designing NIR-absorption materials with small molecular sizes.[46]

Cyclic voltammetry (CV) and differential pulse voltammogram (DPV) measurements for **N-SW-1b**, **N-SW-2** and **N-SW-3** were performed in tetrahydrofuran (THF). As shown in Figure 3c and 3e, **N-SW** series compounds displayed narrower oxidation and reduction behaviours with the extension of non-alternant topologies. More specifically, **N-SW-1b** and **N-SW-2** showed first oxidation potential with irreversible property at 1.33 V and 1.11 V, respectively. **N-SW-3**, however, displayed narrower first oxidation potential with reversible characteristic at 0.86 eV. The first reduction potentials were observed at −0.94 V for **N-SW-1b**, −0.76 V for **N-SW-2** and −0.64 V for **N-SW-3**, respectivelty. The electrical energy levels for the highest occupied molecular orbital (HOMO)/the lowest unoccupied molecular orbital (LUMO) of **N-SW-1b**, **N-SW-2** and **N-SW-3** were calculated to be −5.71 eV/−3.44 eV, −5.49 eV/−3.62 eV and −5.24 eV/−3.74 eV based on the formula ($E_{LUMO/NOMO} = -(E_{onset}^{red}/E_{onset}^{ox} - E_{Fc} + 4.8)$ eV), respectively. Accordingly, the electrochemical energy gaps (E_g^{cv}) of **N-SW-1b**, **N-SW-2** and **N-**

SW-3 were calculated to be 2.27 eV, 1.87 eV and 1.50 eV, respectively.

TD-DFT calculations were carried out to study the electronic characteristics of these **N-SW** series derivatives. Geometry optimization was performed at the B3LYP level with the 6-311G (d,p) basis set using the Gaussian16 package. As shown in Figure 4a, the energy gap of these series of compounds became narrower with extension of π conjugation, from 2.99 eV for **N-SW-1a** to 2.33 eV for **N-SW-3**. The same trend results were also recorded in the UV–Vis absorption and CV analysis. Interestingly, the electron distributions of the HOMO and LUMO of **N-SW-1a** were disparate from those of **N-SW-2** and **N-SW-3**, which might be the cause of their different UV–Vis absorption behaviors. More specifically, for **N-SW-1a**, the HOMO was localized in the azulene unit, and the LUMO was localized in the azulene and pyrrole parts. For **N-SW-2** and **N-SW-3**, however, the HOMO was almost delocalized over the full molecular skeleton, and the LUMO was localized in the azulene units for **N-SW-2** and in the additional pentagon fused two azulene parts (5–7-5–5-7 topological part, Figure 4a) for **N-SW-3**, respectively. These results demonstrated that embedding non-alternant structures such as azulene units could dramatically alter the electronic characteristics of molecules.

Furthermore, the local aromaticity of these **N-SW** series was investigated based on the NICS calculated at the GIAO-RB3LYP/6-311+g (2d, p) level. All the heptagon units in the N-doped S–T–W defect core possessed antiaromatic features (Figure 4b). Interestingly, when one more bond was closed to form a pentagon unit in **N-SW-3**, the aromatic characteristics in the middle azulene unit (D and E rings) dramatically changed compared with those of **N-SW-1a** and **N-SW-2** (Figure 4b). More specifically, the values of D and E rings in **N-SW-2** (D: −19.85 > E: −1.27) and **N-SW-3** (D: −3.82 < E: −11.93) transformed, indicating the breaking of azulene unit properties at these rings in **N-SW-3**, which could be supported by the single crystal analysis results with disparate bond distributions between **N-SW-3** and azulene.[45] In addition, one more antiaromatic ring (J)

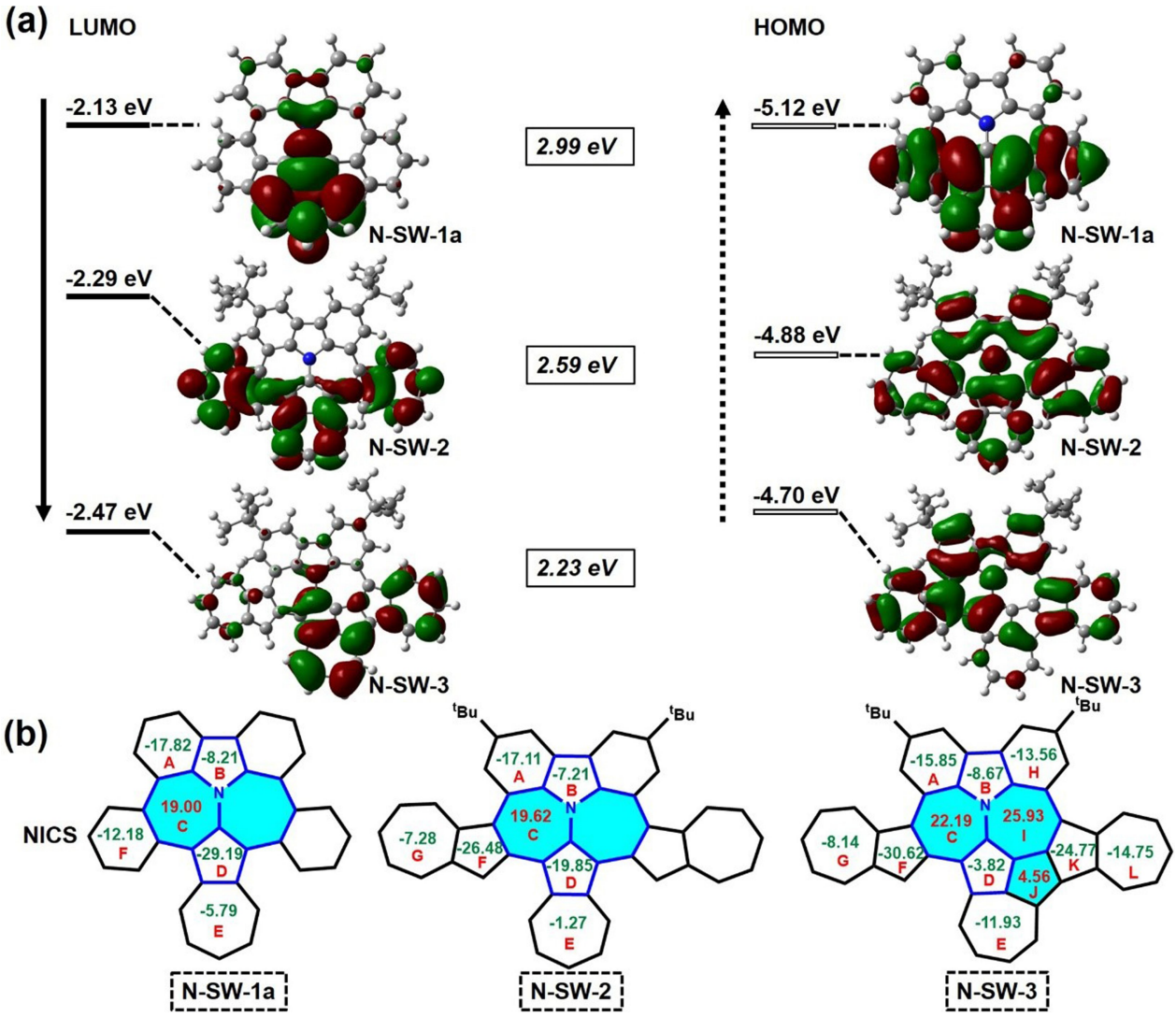

Figure 4. DFT calculations of the **N-SW** series. Molecular orbitals (a) and $NICS(1)_{zz\text{-}avg}$ calculations (b) of **N-SW-1a**, **N-SW-2** and **N-SW-3**.

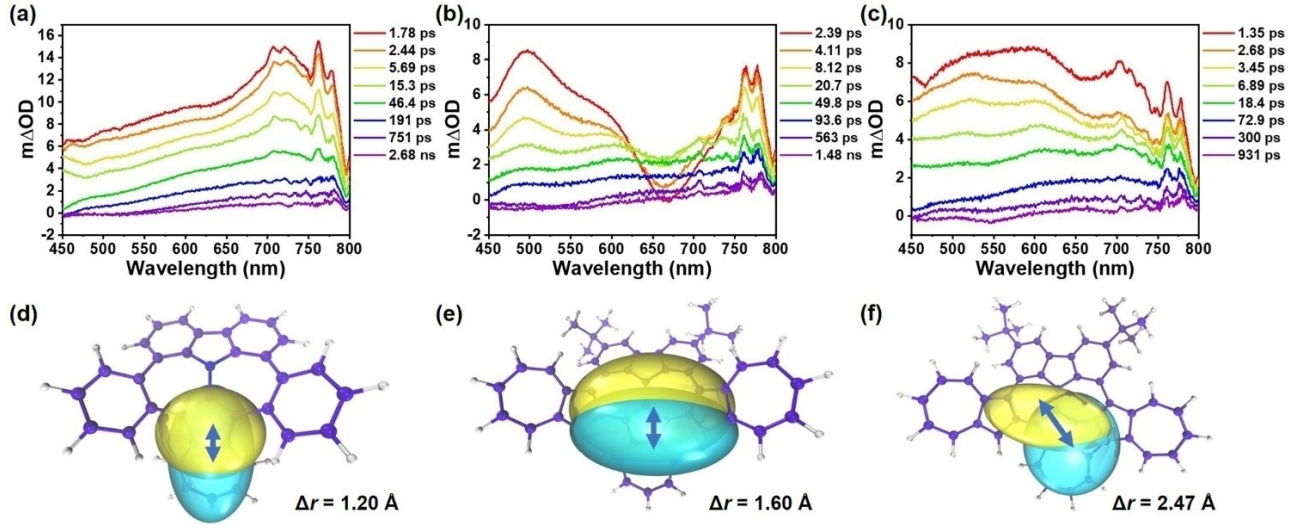

Figure 5. Transient absorption spectra of **N-SW-1 b** (a), **N-SW-2** (b) and **N-SW-3** (c) recorded in DCM. Region of C_{ele} (blue region) and C_{hole} (yellow region), and the Δr indexes of **N-SW-1 a** (d), **N-SW-2** (e) and **N-SW-3** (f) obtained by TD-DFT calculations. The two oval concentrated regions C_{ele} and C_{hole} represented the isosurface of the electron and hole. Δr index represented the distance between the centre of C_{ele} and C_{hole}. The calculation is based on DFT calculations with the help of Multiwfn program.[48]

also appeared in **N-SW-3**. The anisotropy of the induced current density (ACID) was calculated and further supported the local aromaticity of these series of molecules. As shown in Figure S45, for **N-SW-1a** and **N-SW-2**, continuous clockwise diatropic ring currents appeared around the carbazole, benzene and peripheral azulene units in the ACID plots, and counterclockwise paratropic ring currents formed at N-doped heptalene units, which was consistent with the NICS calculations. In **N-SW-3**, continuous counterclockwise paratropic ring currents developed at continuous N-doped heptalenes and one emerging pentagon unit. Carbazole along with three peripheral azulene units showed clockwise diatropic ring currents. All the ACID plots were in agreement with the results from NICS calculations.

The excited state photophysical properties of **N-SW-1b**, **N-SW-2** and **N-SW-3** were investigated in DCM by femtosecond transient absorption (*fs*-TA) spectroscopy upon 267 nm excitation. As shown in Figure 5a–c, the spectra of these three molecules presented a broad band at approximately 450–800 nm after excitation, and subsequently decay to baseline within nanosecond scale. Noticed that a unique descending peak at 600 nm was recorded for **N-SW-2** (Figure 5b), which could contribute to the accumulation of excited state absorption (ESA) and ground-state bleaching (GSB) signals referring to the steady state UV/Vis absorption spectrum (Figure 3a). To further investigate the transient species involved in the decay pathway of these molecules, kinetic fitting at 600 nm was conducted for the spectra of them (Figure S42), and found that the excited-state lifetimes for **N-SW-1b**, **N-SW-2**, and **N-SW-3** are 403.5 ps, 424.7 ps, and 513.0 ps, respectively. Such short lifetimes indicate that there are almost no triplet species generated for these three molecules. Moreover, it is also impossible for these molecules to deactivate via internal conversion since the lifetime scale is not matched according to our previous study.[6a] Meanwhile, the charge separation is clearly observed in the electron-hole distribution for S_0–S_1 transition (Figure 4 and Figure 5), so this excited state lifetime could be attributed to the charge separation state. The extent of the charge separation, which can be evaluated by the Δr index (Figure 5d–f),[47] greatly affects the time for charge recombination. With the largest degree of charge separation ($\Delta r = 2.47$ Å, Figure 5f), **N-SW-3** possesses the longest excited state lifetime, followed by the **N-SW-2** ($\Delta r =$ 1.60 Å, Figure 5e) and **N-SW-1** ($\Delta r = 1.20$ Å, Figure 5d). It is obvious that the existence of the ring J (the extra pentagon) in **N-SW-3** breaks the symmetry of the structure, causing more electron locating on it after excitation and further enlarging the degree of charge separation, which eventually prolongs the excited state lifetime. In conclusion, all these three molecules could generate a charge separation state upon excitation, and the **N-SW-3** possesses the greatest rate constant for charge recombination than the other two molecules. This is likely due to **N-SW-3** has the largest Δr index, which resulted from its asymmetric structure.

Conclusion

In summary, we successfully synthesized three nanographenes with N-doped non-alternant topologies by direct arylation. Among them, to our best knowledge, **N-SW-3** is the largest N-doped non-benzenoid molecule to date. Single-crystal analysis showed **N-SW-1a** and **N-SW-2** displayed alternant bond length distributions in the N-doped heptagons. **N-SW-3**, however, was divergent, with one more antiaromatic pentagon fused and asymmetry of the N-doped heptagons, which resulted in completely different physicochemical properties compared with **N-SW-1a** and **N-SW-2**. UV–Vis absorption spectra analysis showed that the onset

peaks of **N-SW-2** and **N-SW-3** were prolonged up to 900 nm in the near-infrared region, which was much longer than that of similarly sized N-doped nanographene with six-membered rings (**8b**,[42] Figure 1c, around 600 nm), thus showing the narrower energy gaps. The high stability of these **N-SW** series under ambient conditions with a narrower energy gap indicated that the incorporation of non-alternant topology into nanographenes might be a reasonable strategy for designing NIR-absorption materials with small molecular sizes.[46] Our work reported herein offers a feasible way to bottom-up fabricate larger N-doped non-alternant conjugation systems, and provides fundamental insights into the chemical, optical and electric properties of novel N-doped nanographenes with non-alternant topologies.

Acknowledgements

This work was supported by the Hong Kong Research Grants Council (27301720, 17304021), National Natural Science Foundation of China (No.: 22122114). J. L. is grateful for the funding from The University of Hong Kong (HKU) and ITC to the SKL. We thank the UGC funding administered by HKU for supporting the Time-of-Flight Mass Spectrometry Facilities under the Support for Interdisciplinary Research in Chemical Science. We acknowledge the computer cluster (HPC2021) of HKU for gen-erous allocations of computer resources.

Conflict of Interest

The authors declare no conflict of interest.

Data Availability Statement

The data that support the findings of this study are available in the supplementary material of this article.

Keywords: Antiaromaticity. · Azupyrene · N-Doping · Nanographenes · Non-Alternant Topologies

[1] V. M. Tsefrikas, L. T. Scott, *Chem. Rev.* **2006**, *106*, 4868–4884.
[2] T. Amaya, T. Hirao, *Chem. Rec.* **2015**, *15*, 310–321.
[3] a) X. Yang, D. Liu, Q. Miao, *Angew. Chem. Int. Ed.* **2014**, *53*, 6786–6790; b) Q. Miao, *Chem. Rec.* **2015**, *15*, 1156–1159; c) K. Y. Cheung, X. Xu, Q. Miao, *J. Am. Chem. Soc.* **2015**, *137*, 3910–3914; d) S. H. Pun, Q. Miao, *Acc. Chem. Res.* **2018**, *51*, 1630–1642; e) S. H. Pun, Y. Wang, M. Chu, C. K. Chan, Y. Li, Z. Liu, Q. Miao, *J. Am. Chem. Soc.* **2019**, *141*, 9680–9686; f) Y. Zhang, S. H. Pun, Q. Miao, *Chem. Rev.* **2022**, *122*, 14554–14593.
[4] a) I. R. Márquez, N. Fuentes, C. M. Cruz, V. Puente-Muñoz, L. Sotorrios, M. L. Marcos, D. Choquesillo-Lazarte, B. Biel, L. Crovetto, E. Gómez-Bengoa, M. T. González, R. Martin, J. M. Cuerva, A. G. Campaña, *Chem. Sci.* **2017**, *8*, 1068–1074; b) I. R. Márquez, S. Castro-Fernández, A. Millán, A. G. Campaña, *Chem. Commun.* **2018**, *54*, 6705–6718; c) C. M. Cruz, I. R. Márquez, I. F. A. Mariz, V. Blanco, C. Sánchez-Sánchez, J. M. Sobrado, J. A. Martín-Gago, J. M. Cuerva, E. Maçôas, A. G. Campaña, *Chem. Sci.* **2018**, *9*, 3917–3924; d) C. M. Cruz, S. Castro-Fernández, E. Maçôas, J. M. Cuerva, A. G. Campaña, *Angew. Chem. Int. Ed.* **2018**, *57*, 14782–14786; e) C. M. Cruz, I. R. Márquez, S. Castro-Fernández, J. M. Cuerva, E. Maçôas, A. G. Campaña, *Angew. Chem. Int. Ed.* **2019**, *58*, 8068–8072; f) M. A. Medel, R. Tapia, V. Blanco, D. Miguel, S. P. Morcillo, A. G. Campaña, *Angew. Chem. Int. Ed.* **2021**, *60*, 6094–6100; g) M. A. Medel, C. M. Cruz, D. Miguel, V. Blanco, S. P. Morcillo, A. G. Campaña, *Angew. Chem. Int. Ed.* **2021**, *60*, 22051–22056; h) J. P. Mora-Fuentes, M. D. Codesal, M. Reale, C. M. Cruz, V. G. Jiménez, A. Sciortino, M. Cannas, F. Messina, V. Blanco, A. G. Campaña, *Angew. Chem. Int. Ed.* **2023**, *62*, e202301356.
[5] a) K. Kawasumi, Q. Zhang, Y. Segawa, L. T. Scott, K. Itami, *Nat. Chem.* **2013**, *5*, 739–744; b) S. Matsubara, Y. Koga, Y. Segawa, K. Murakami, K. Itami, *Nat. Catal.* **2020**, *3*, 710–718; c) Chaolumen, I. A. Stepek, K. E. Yamada, H. Ito, K. Itami, *Angew. Chem. Int. Ed.* **2021**, *60*, 23508–23532; d) I. A. Stepek, M. Nagase, A. Yagi, K. Itami, *Tetrahedron* **2022**, *123*, 132907; e) G. González Miera, S. Matsubara, H. Kono, K. Murakami, K. Itami, *Chem. Sci.* **2022**, *13*, 1848–1868.
[6] a) Y. Fei, Y. Fu, X. Bai, L. Du, Z. Li, H. Komber, K.-H. Low, S. Zhou, D. L. Phillips, X. Feng, J. Liu, *J. Am. Chem. Soc.* **2021**, *143*, 2353–2360; b) Y. Fei, J. Liu, *Adv. Sci.* **2022**, *9*, 2201000; c) J. Wang, F. G. Gámez, J. Marín-Beloqui, A. Diaz-Andres, X. Miao, D. Casanova, J. Casado, J. Liu, *Angew. Chem. Int. Ed.* **2023**, *62*, e202217124.
[7] a) A. Konishi, M. Yasuda, *Chem. Lett.* **2021**, *50*, 195–212; b) K. Horii, R. Kishi, M. Nakano, D. Shiomi, K. Sato, T. Takui, A. Konishi, M. Yasuda, *J. Am. Chem. Soc.* **2022**, *144*, 3370–3375; c) A. Konishi, K. Horii, M. Hirose, M. Yasuda, *Pure Appl. Chem.* **2023**, *95*, https://doi.org/10.1515/pac-2023-0117; d) A. Konishi, K. Horii, M. Yasuda, *J. Phys. Org. Chem.* **2023**, *36*, e4495.
[8] a) X. Yang, M. Hoffmann, F. Rominger, T. Kirschbaum, A. Dreuw, M. Mastalerz, *Angew. Chem. Int. Ed.* **2019**, *58*, 10650–10654; b) X. Yang, F. Rominger, M. Mastalerz, *Angew. Chem. Int. Ed.* **2019**, *58*, 17577–17582; c) T. Kirschbaum, F. Rominger, M. Mastalerz, *Angew. Chem. Int. Ed.* **2020**, *59*, 270–274.
[9] a) J. M. Fernández-García, P. J. Evans, S. Medina Rivero, I. Fernández, D. García-Fresnadillo, J. Perles, J. Casado, N. Martín, *J. Am. Chem. Soc.* **2018**, *140*, 17188–17196; b) J. Urieta-Mora, M. Krug, W. Alex, J. Perles, I. Fernández, A. Molina-Ontoria, D. M. Guldi, N. Martín, *J. Am. Chem. Soc.* **2020**, *142*, 4162–4172.
[10] a) J. Liu, S. Mishra, C. A. Pignedoli, D. Passerone, J. I. Urgel, A. Fabrizio, T. G. Lohr, J. Ma, H. Komber, M. Baumgarten, C. Corminboeuf, R. Berger, P. Ruffieux, K. Müllen, R. Fasel, X. Feng, *J. Am. Chem. Soc.* **2019**, *141*, 12011–12020; b) J. Ma, Y. Fu, E. Dmitrieva, F. Liu, H. Komber, F. Hennersdorf, A. A. Popov, J. J. Weigand, J. Liu, X. Feng, *Angew. Chem. Int. Ed.* **2020**, *59*, 5637–5642; c) T. G. Lohr, J. I. Urgel, K. Eimre, J. Liu, M. Di Giovannantonio, S. Mishra, R. Berger, P. Ruffieux, C. A. Pignedoli, R. Fasel, X. Feng, *J. Am. Chem. Soc.* **2020**, *142*, 13565–13572.
[11] A. Ong, T. Tao, Q. Jiang, Y. Han, Y. Ou, K.-W. Huang, C. Chi, *Angew. Chem. Int. Ed.* **2022**, *61*, e202209286.
[12] G. Dai, J. Chang, J. Luo, S. Dong, N. Aratani, B. Zheng, K.-W. Huang, H. Yamada, C. Chi, *Angew. Chem. Int. Ed.* **2016**, *55*, 2693–2696.
[13] G. Dai, J. Chang, W. Zhang, S. Bai, K.-W. Huang, J. Xu, C. Chi, *Chem. Commun.* **2015**, *51*, 503–506.
[14] X. S. Zhang, Y. Y. Huang, J. Zhang, W. Meng, Q. Peng, R. Kong, Z. Xiao, J. Liu, M. Huang, Y. Yi, L. Chen, Q. Fan, G.

Lin, Z. Liu, G. Zhang, L. Jiang, D. Zhang, *Angew. Chem. Int. Ed.* **2020**, *59*, 3529–3533.
[15] H. Xin, J. Li, R. Q. Lu, X. Gao, T. M. Swager, *J. Am. Chem. Soc.* **2020**, *142*, 13598–13605.
[16] A. G. Anderson Jr, A. A. MacDonald, A. F. Montana, *J. Am. Chem. Soc.* **1968**, *90*, 2993–2994.
[17] A. G. Anderson Jr, A. F. Montana, A. MacDonald, G. M. Masada, *J. Org. Chem.* **1973**, *38*, 1445–1450.
[18] H. Reel, E. Vogel, *Angew. Chem. Int. Ed.* **1972**, *11*, 1013–1014.
[19] S. Das, J. Wu, *Org. Lett.* **2015**, *17*, 5854–5857.
[20] X. Lu, Z. Chen, P. v R Schleyer, *J. Am. Chem. Soc.* **2005**, *127*, 20–21.
[21] C. Y. Won, N. R. Aluru, *J. Am. Chem. Soc.* **2008**, *130*, 13649–13652.
[22] S. Bhowmick, U. V. Waghmare, *Phys. Rev. B* **2010**, *81*, 155416.
[23] H. Sahin, J. Sivek, S. Li, B. Partoens, F. M. Peeters, *Phys. Rev. B* **2013**, *88*, 045434.
[24] G.-L. Chai, Z. Hou, D.-J. Shu, T. Ikeda, K. Terakura, *J. Am. Chem. Soc.* **2014**, *136*, 13629–13640.
[25] Y. An, A. F. Oliveira, T. Brumme, A. Kuc, T. Heine, *Adv. Mater.* **2020**, *32*, 2002442.
[26] B. P. Klein, L. Ruppenthal, S. J. Hall, L. E. Sattler, S. M. Weber, J. Herritsch, A. Jaegermann, R. J. Maurer, G. Hilt, J. M. Gottfried, *ChemPhysChem* **2021**, *22*, 1065–1073.
[27] A. Konishi, K. Horii, D. Shiomi, K. Sato, T. Takui, M. Yasuda, *J. Am. Chem. Soc.* **2019**, *141*, 10165–10170.
[28] P. Mathey, F. Lirette, I. Fernández, L. Renn, R. T. Weitz, J.-F. Morin, *Angew. Chem. Int. Ed.* **2023**, *62*, e202216281.
[29] X. Wang, G. Sun, P. Routh, D.-H. Kim, W. Huang, P. Chen, *Chem. Soc. Rev.* **2014**, *43*, 7067–7098.
[30] X.-K. Kong, C.-L. Chen, Q.-W. Chen, *Chem. Soc. Rev.* **2014**, *43*, 2841–2857.
[31] H. Wang, T. Maiyalagan, X. Wang, *ACS Catal.* **2012**, *2*, 781–794.
[32] M. D. Tzirakis, M. Orfanopoulos, *Chem. Rev.* **2013**, *113*, 5262–5321.
[33] M. Stepien, E. Gonka, M. Zyla, N. Sprutta, *Chem. Rev.* **2017**, *117*, 3479–3716.
[34] A. Borissov, Y. K. Maurya, L. Moshniaha, W. S. Wong, M. Zyla-Karwowska, M. Stepien, *Chem. Rev.* **2022**, *122*, 565–788.
[35] H. Luo, J. Liu, *Angew. Chem. Int. Ed.* **2023**, e202302761.
[36] S. Mishra, M. Krzeszewski, C. A. Pignedoli, P. Ruffieux, R. Fasel, D. T. Gryko, *Nat. Commun.* **2018**, *9*, 1714.
[37] M. Krzeszewski, Ł. Dobrzycki, A. L. Sobolewski, M. K. Cyrański, D. T. Gryko, *Angew. Chem. Int. Ed.* **2021**, *60*, 14998–15005.
[38] M. Krzeszewski, Ł. Dobrzycki, A. L. Sobolewski, M. K. Cyrański, D. T. Gryko, *Chem. Sci.* **2023**, *14*, 2353–2360.
[39] S. C. Gadekar, B. K. Reddy, S. P. Panchal, V. G. Anand, *Chem. Commun.* **2016**, *52*, 4565–4568.
[40] H. Yokoi, Y. Hiraoka, S. Hiroto, D. Sakamaki, S. Seki, H. Shinokubo, *Nat. Commun.* **2015**, *6*, 8215.
[41] S. Ito, Y. Tokimaru, K. Nozaki, *Angew. Chem. Int. Ed.* **2015**, *54*, 7256–7260.
[42] Y. Tokimaru, S. Ito, K. Nozaki, *Angew. Chem. Int. Ed.* **2018**, *57*, 9818–9822.
[43] M. Murai, S. Iba, H. Ota, K. Takai, *Org. Lett.* **2017**, *19*, 5585–5588.
[44] Deposition numbers 2254357 (for **N-SW-1a**), 2254356 (for **N-SW-2**) and 2254355 (for **N-SW-3**) contain the supplementary crystallographic data for this paper. These data are provided free of charge by the joint Cambridge Crystallographic Data Centre and Fachinformationszentrum Karlsruhe Access Structures service.
[45] B. Dittrich, F. P. A. Fabbiani, J. Henn, M. U. Schmidt, P. Macchi, K. Meindl, M. A. Spackman, *Acta Crystallogr. Sect. B* **2018**, *74*, 416–426.
[46] Y. Tanaka, N. Fukui, H. Shinokubo, *Nat. Commun.* **2020**, *11*, 3873.
[47] J. Li, S. Yang, Z. Deng, S. Ni, S. Chen, L. Dang, M. D. Li, *Phys. Chem. Chem. Phys.* **2022**, *24*, 14623–14630.
[48] T. Lu, F. Chen, *J. Comput. Chem.* **2012**, *33*, 580–592.

Manuscript received: May 16, 2023
Accepted manuscript online: July 8, 2023
Version of record online: ■■, ■■

Research Articles

Nanographenes

C. Wang, Z. Deng, D. L. Phillips, J. Liu* ——— e202306890

Extension of Non-alternant Nanographenes Containing Nitrogen-Doped Stone-Thrower-Wales Defects

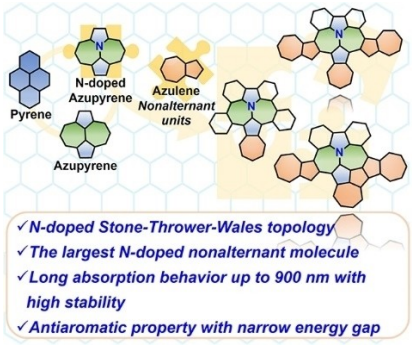

Saddle-shaped nanographenes containing N-doped Stone-Thrower-Wales topological defects have been synthesized that possess much narrower energy gaps than similar-sized N-doped nanographenes with six-membered rings. This work indicates that the introduction of non-alternant topologies is an efficient way to narrow the energy gap without extending the molecular size.